A Study on Central Crack Formation in Cross Wedge Rolling

Xianyan Zhou[a], Zhutao Shao[a], Catalin I. Pruncu[a], Lin Hua[b], Daniel Balint[a], Jianguo Lin[a], Jun Jiang[a,*]

a. Department of Mechanical Engineering, Imperial College London, Exhibition Road, London SW7 2AZ, the UK

b. School of Automotive Engineering, Wuhan University of Technology, Luoshi Road, Wuhan 430070, China

Abstract

Cross wedge rolling (CWR) is an innovative roll forming process, used widely in the transportation industry. It has high production efficiency, consistent quality and efficient material usage. However, the continual occurrence of crack formation in the centre of the workpiece is a critical problem excluding the CWR technique from more safety-critical applications, in particular, aerospace components. The mechanisms of central fracture formation are still unclear because of a combination of complicated stress and strain states at various stages of CWR. Thus, the aim of this study is to understand the stress/strain distribution and evolution during the CWR process and identify the key variables which determine central crack formation. A comprehensive investigation was then conducted to simulate 27 experimental cases. The stress and strain distributions in the workpiece were evaluated by finite element analysis. Various damage models from literature were applied and compared. A new fracture criterion was proposed, which was able to successfully determine the central crack formation in all 27 experimental cases. This criterion can be applied in CWR tool and process design, and the enhanced understanding may enable the adoption of CWR by the aerospace industry.

Keywords: **Cross wedge rolling; central cracking; fracture mechanism; fracture criterion.**

*Corresponding author.
Email address: jun.jiang@imperial.ac.uk (J. Jiang)

1. Introduction

The cross wedge rolling is an innovative metal forming process designed to efficiently produce axisymmetric or cylindrical parts and preforms, in which billets are finished as axisymmetric profiles using wedged tools moving tangentially relative to each other as described by Fu and Dean (1993). CWR produces near-net-shaped parts, and its benefits (i.e. high throughput, efficient material usage, excellent part mechanical properties and lower environmental impact) make it favourable compared to some conventional manufacturing processes. CWR has been used successfully in extensive applications, including the production of large and elongated parts (e.g. stepped axles and shafts) and in die-forging preforms (i.e. double-ended spanners, connecting rods, forks and bicycle pedal cranks) as reviewed by Hu et al. (1995, 2018) and Pater (2014). Hu et al. (2012) highlighted that more than 300 production lines have been established worldwide with an estimated production value of greater than $200 million per year.

Over the last five decades, CWR has been investigated comprehensively to improve its performance. Although considerable understanding of the CWR process has been gained through prior research, the central crack formation mechanism remains an unsolved problem. Central cracks, also called the Mannesmann hole defect as mentioned by Lee et al. (2008), are internal voids/cracks that form in the middle (both axially and radially) of the workpiece during CWR. Both Li et al. (2002) and Yang et al. (2018) observed in experiments that the central crack is ductile in nature. An increasing number of fracture criteria and damage models have been developed and applied to predict ductile fracture in engineering application. For example, Rice and Tracey model proposed by Rice and Tracey (1969), represented the voids growth with the consideration of stress triaxiality. As a good example of micromechanics based damage models, this model is still widely used due to its simplicity. Gurson (1977), based on the Rice and Tracey model, employed a new term, voids density, to describe the effects of damage caused by the voids on the material strength. Later Needleman and Tvergaard (1984) improved the model with the consideration the voids nucleation and coalescence. Many further modifications were made by considering the effects of other factors, such as voids size by Wen and Huang (2005), shape by Madou and Leblond (2012) and shear effects by Nahshon and Hutchinson (2008). Continuum damage mechanics (CDM) models consider the effects of damage on the material constitutive relationships. For example, Lemaitre (1985) introduced the softening effect caused by damage to the flow law. Phenomenological ductile fracture models, based on massive experimental data, are studied intensively, which accumulate the plastic strain with the consideration of stress states. Wierzbicki et al. (2005) introduced the stress triaxiality into seven fracture criteria, the application ranges of which were determined. Xue and Wierzbicki (2008)

incorporated both the stress triaxiality and Lode parameters into a damage model, and higher prediction accuracy was gained. The robustness and application range of various phenomenological models were investigated by Cao et al. (2015). These models are applicable to a wide range of stress states. However, many of them are restricted to a specific processing condition of an industrial application and due to a large number of material constants in these models, and their determination and calibration is time-consuming and costly.

Various models have been introduced or proposed to predict central crack formation in the CWR. Li and Lovell (2004) compared the Von Mise stress, the mean stress and the plastic strain based on a combined numerical and experimental approach with different materials, pure aluminium, copper and steels, and found the plastic strain was the best criterion to predict the internal defects, which was agreed by Lee et al. (2008) through comparing the damage value with the crack condition observed in the experiment of the cold CWR with micro-alloyed steels SHCW80. The Cockcroft–Latham model was applied by Pater (2014) to study the effect of geometrical parameters on the internal cracking based on the validation that the damage value of the central point was higher than that of another point far from the central point in the condition of hot working with the billet material steels C45. Nevertheless, Zhou et al. (2014) conducted the simulation of the multi-wedge CWR process for forming stepped shafts with the billet AISI 5140, and found the Cockcroft–Latham damage values at different locations on the workpiece did not match the cracking statuses from the experimental observation. Mirahmadi et al. (2014) applied the normalized Cockcroft–Latham model to predict the internal cracking in CWR of Nimonic® 80A and Nimonic® 115 superalloys and validated the model by the finding that the damage distribution from FE modelling was similar with the cracking morphology form the experimental observation. Novella et al. (2015) modified the Oyane damage model by taking the effects of temperature and strain rate into consideration and validated the model by comparing the fracture location predicted by the FE modelling with the experimental observation. Recently, A new experimental method was developed by Komischke et al. (2018) and proved that the Mohr-Coulomb criterion was accurate in predicting the internal fracture in skew rolling. Pater et al. (2019) compared nine damage models with the rotation compression test and determined the damage models for predicting the crack formation under certain stress states. Although lots of progress has been done in predicting the central crack formation in the CWR, most of the models were not validated quantitatively and the best criterion for central crack prediction cannot be agreed. Therefore, it is necessary to develop a robust damage model or fracture criterion to predict the central crack formation with a high accuracy and to be widely adopted by the industry.

Causes for central cracks in the CWR have been widely discussed in literature. Fu and Dean (1993) reviewed that central cracks might result from the cumulative effect of alternating normal stress and shear stress in the central region of the billet, loading cycles, torsions between different layers on the workpiece and large inclusions present there. When the material related factors are taken into account, the temperature and strain rates have great effects in central crack formation as investigated in the research of Li (2003) and Novella et al. (2015), which involve many other microstructure evolution such as phase transformation, precipitate, recrystallization, defect formation (carbides) and oxidation. Currently, it is generally believed that the tool parameters take the dominant role in forming central cracks mainly because they affect the stress strain states in the workpiece, which can be found in many publications on the effects of tool geometries on the central crack formation, e.g. (Li and Lovell, 2004; Pater, 2014; Pater et al., 2019; Yamane et al., 2019; Yang et al., 2018). Thus, this research aims to understand the stress strain state, how they evolve and lead to fracture during the CWR process.

Great progresses have been made in understanding how the stress states affect the central crack formation. Li et al. (2002) proposed that the combination of the shear and the tensile stress might be the dominant factor causing central crack formation by analysing the morphologies of central cracks in pure Aluminium alloys. Yang et al. (2018) supported this opinion by investigating the shear deformation and normal deformation in the simulation of the rolling process of the steels AISI 1045 at 1100 °C. Recently, Yamane et al. (2019) conducted skew rolling experiments along with the FE modelling and also concluded the combined effects of tensile stress and shear stress caused the formation of internal fracture. However, these two dominant items, particularly, the shear stress, were not well presented in the previous damage models or fracture criteria. Pater et al. (2019) suggested that the maximum shear stress criterion may be applied under certain stress states. Therefore, to achieve the high accuracy in predicting the central cracks, further understanding of the specific fracture mechanisms in central cracks is required.

This research aims to understand the stress strain states, and the evolution and how they lead to fracture during the CWR process. To purely focus on the study of stress strain states without the influence of other potential variables for central cracks, the experimental data from the previous study by Li et al. (2002) and Li (2003) with pure aluminium at room temperature was investigated, during which the stress strain states vary systematically by rigorously controlling and changing the geometrical parameters systematically. Based on this set of rigorous experimental studies, 27 FE models of distinct CWR die shapes were created to interrogate the

stress-strain behaviour. The modelling methodology is presented in Section 2 including FE modelling, experimental data and the proposal of the new fracture criterion. Section 3 contains in-depth stress and damage analysis of the data extracted from the FE modelling, and insights into the fracture mechanism.

2. Methodology

2.1 Finite element model

The rolling process was simulated using a commercial FE software, QForm[1] VX8.2.4, which is particularly suitable for modelling large thermal-mechanical deformation; mainly due to its advanced meshing algorithms (e.g. dual mesh method) which can effectively improve the computational speed and avoid the convergence problem as indicated by Stebunov et al. (2011).

As shown in Fig. 1(a), due to the symmetrical nature of the process and for the sake of computational efficiency, only the left-hand side of the CWR model was modelled. Initially, the workpiece is placed in the middle of two guide plates, and two rollers. During processing, the workpiece rotates along its axial shaft driven by the two rollers, rotating in the same direction with the same linear rotational speed. Two guide plates maintain the workpiece being in the middle position. Fig. 1(b) shows the geometry of the tools. The wedge is normally divided into four zones: knifing, guiding, stretching and sizing. Three important geometrical parameters are defined including the forming angle α, stretching angle β and area reduction ratio η, defined as $1 - ({}^{d}/_{d_0})^2$. It is noted that the die geometry is different with the description in experimental data published by Li et al. (2002) where flat dies were applied, in order to keep consistent with the practical applications and the latest research to allow our criterion to be transferred and reached by a broader practical CWR community. Meanwhile, it was investigated that the effect of die geometries (roller or flat dies) on stress strain states is minimal due to the low ratio of the workpiece diameter (25.4 mm) to the die diameter (500 mm), at 0.05. The materials for the workpiece and dies are commercial pure aluminium AA1100 and tool steel 1045, respectively. The visco-plastic behaviour of Al 1100 was considered in this numerical study, though the time-dependent part (strain rate hardening) is very small at room temperature in this case. Also, due to the extensively large plastic deformation (>100%), it is not unreasonable to ignore the elastic strain. The final constitutive relationship ("Theoretical basis of QForm," 2017) is shown in Eq. 1, where the deformation rate is related to the stress deviator σ'_{ij}:

[1] http://www.qform3d.co.uk

$$\dot{\varepsilon}_{ij} = \frac{3}{2}\frac{\dot{\bar{\varepsilon}}}{\bar{\sigma}} \cdot \sigma'_{ij} \quad (1)$$

where $\bar{\sigma}$ is the effective stress, $\dot{\bar{\varepsilon}}$ is the effective deformation rate, $\dot{\varepsilon}_{ij}$ is the strain rate tensor and σ'_{ij} is the stress deviator.

The classic Coulomb friction model was employed to define the contact interaction between the workpiece and dies based on its static friction nature. The friction coefficient between the workpiece and dies was set at 0.6. Meanwhile, the friction coefficient between the workpiece and the guide plates was assumed to be zero, as these guide plates were only used to keep the workpiece in place. The friction model and friction coefficient used in the FE simulation, were validated experimentally by comparing the final diameter of the CWR formed part between the FE model (22.72 mm) and the experimental one (22.97 mm).

The explicit integration method was employed because of its high efficiency and accuracy in solving severe plastic deformation problems. A dual mesh strategy was applied, for which the region of interest, the central area along the axial direction, was continuously refined with an adaption factor of 2 during the rolling process to ensure high accuracy of the stress and strain calculations. For example, the number of elements increased from an initial value of 21991 to over 70000 at the end of the CWR.

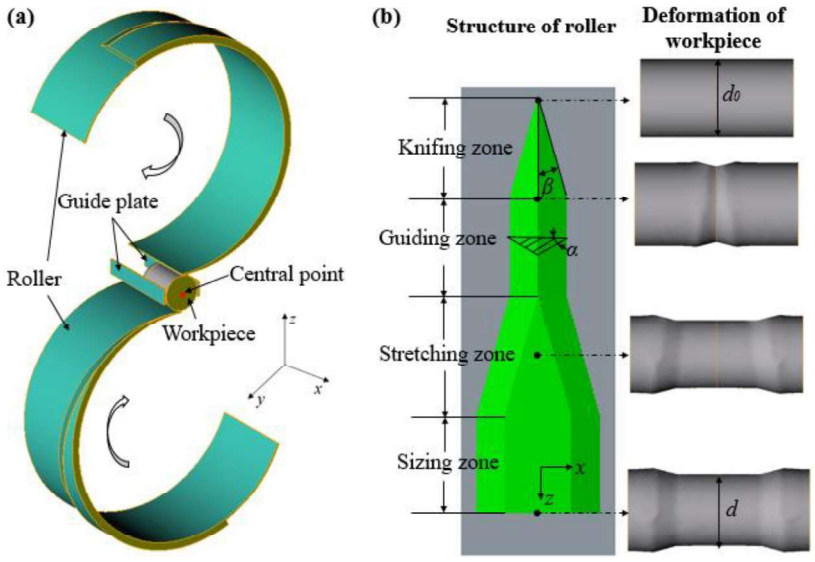

Fig. 1. The configuration of CWR (a) schematic of the modelled CWR process (b) configuration of the roller and the corresponding deformation stages during CWR.

2.2 Experimental data

A rigorous experimental study on the central crack formation of commercially pure aluminium (Al 1100) was carried out previously at room temperature by systematically varying three key die geometry parameters, i.e. the forming angle α, stretching angle β and area reduction ratio η, as illustrated in Fig. 1(b). The summary of the detailed experimental study is presented in Table 1. In total, 27 cases were studied with 12 cracked and 15 without central cracks; 27 FE models were created to explicitly replicate the variation of die geometries, with the aim to investigate the stress and strain variations and subsequent central cracking mechanisms. More details of the process parameters can be found in the study of Li (2003) and/or Li et al. (2002).

Table 1.

Results of 27 CWR experiments considering various geometrical parameters (Li, 2003; Li et al., 2002).

Case Number	η	β (°)	α (°)	Experimental results
1	27	3	15	No crack
2	27	5	15	Central crack
3	27	7	15	Central crack
4	35	3	15	No crack
5	35	5	15	Central crack
6	35	7	15	Central crack
7	44	3	15	No crack
8	44	5	15	Central crack
9	44	7	15	Central crack
10	27	3	20	No crack
11	27	5	20	Central crack
12	27	7	20	Central crack
13	35	3	20	No crack
14	35	5	20	Central crack
15	35	7	20	Central crack
16	44	3	20	No crack
17	44	5	20	Central crack
18	44	7	20	Central crack
19	27	3	30	No crack
20	27	5	30	No crack
21	27	7	30	No crack
22	35	3	30	No crack
23	35	5	30	No crack
24	35	7	30	No crack
25	44	3	30	No crack
26	44	5	30	No crack
27	44	7	30	No crack

2.3 A new fracture criterion for predicting central crack formation

2.3.1 Proposal of a new fracture criterion

A new central crack formation criterion is proposed in this study. This criterion considers the effects of the maximum shear stress (τ_m) and the first principal stress (σ_1). It effectively combines the Tresca and first

principal stress fracture criterion. The proposed criterion is described by Eq. (2), where D represents the damage value and D_f is the critical damage value causing fracture. Once D exceeds D_f in the central region, the workpiece is predicted to fracture there.

$$D = A\,\tau_m + B\sigma_1 \begin{cases} \geq D_f & \text{Central Crack} \\ < D_f & \text{No crack} \end{cases} \tag{2}$$

To apply this criterion for various materials, constants A and B are used. A linear relationship between the effect of maximum shear stress and the first principal stress to fracture was defined as $A + B = 1$, allowing to reduce the number of material constants. Then, the proposed fracture criterion was rewritten as Eq. (3).

$$D_n = \left(\frac{A}{D_f}\right)\tau_m + \left(\frac{1-A}{D_f}\right)\sigma_1 \begin{cases} \geq 1 & \text{Central Crack} \\ < 1 & \text{No crack} \end{cases} \tag{3}$$

2.3.2 Mechanistic basis of the fracture criterion

The proposed damage model considers the classic Tresca and the first principal stress fracture criterion, both of which were carefully compared and discussed by Yu (2002). It is well known that the Tresca criterion can predict ductile fracture, while the first principal stress theory is more suitable for predicting brittle fracture. Li et al. (2014) discovered that the Tresca criterion is accurate for predicting the case of pure shear, but not accurate when normal stress is applied. This is because pure shear mode and the uniaxial extension are led by two different fracture mechanisms and these two fracture mechanisms are not independent under a multiaxial stress state but interact with each other. In the present study that simulates the CWR routine, the central region of the workpiece was subjected to triaxial stresses, with principal stress varying among a wide range, whereas the maximum shear stress is accumulating during the whole process. Thus, the interaction and combined effects of the normal stress and the shear stress are considered to determine the damage progress.

The Eq. (2) describes the proposed fracture criterion and considers the fact that under triaxial stress states, both the axial stress and shear stress are important to generate fracture. If the material is ideally brittle (no evidence of plastic deformation during the fracture process), A = 0, and the new damage model is reduced to the maximum principal stress theory with B = 1. Whereas, when the material is extremely ductile, B can be regarded as 0, and the new model is reduced to the maximum shear stress criterion with A = 1. However, as for general materials, they possess some resistances to both shear stress and normal stress. If the material behaviour is resistant to normal stress and is weak under shear stress, the fracture mechanism is a shear dominant fracture. Thus, A will be positive and larger than B. If B is positive, it means that the normal stress has a positive effect on

the shear dominant fracture. If B is zero, it means the normal stress has no effect on the fracture. Otherwise, it has a negative effect and restrains the fracture. This law also applies for B. If B is larger than A, it will be a normal stress dominant fracture, positive A accelerates the fracture and negative A constrains the fracture.

Fig. 2 illustrates the fracture locus of the maximum principal stress theory (two vertical dashed lines), Tresca criterion (horizontal dashed line) and the proposed model (two solid lines). Nonetheless, neither the maximum principal stress or the Tresca criterion considers the interaction between the normal stress and shear stress and their combined effects on fracture, which are now considered in the new criterion as indicated by the Eq. (2) and (3). Note that only the domain above σ axle is discussed because the maximum shear stress ($\tau_m = {(\sigma_1 - \sigma_3)}/{2}$) is equal or over zero. $\sigma_{f,t}$ and $\sigma_{f,c}$ present the ultimate strength in uniaxial tension and compression respectively.

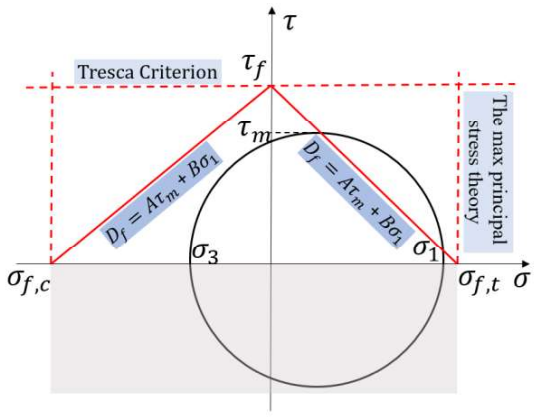

Fig. 2. Representation of fracture locus by the proposed criterion using the fracture lines and Mohr's circle.

The new model can also be presented as the following to keep consistent with the Tresca criterion and the first principal stress theory:

$$\begin{cases} \sigma_{f,t}\tau_m + \tau_f\sigma_1 = \sigma_{f,t}\tau_f & (\sigma_1 \geq 0) \\ \sigma_{f,c}\tau_m + \tau_f\sigma_1 = \sigma_{f,c}\tau_f & (\sigma_1 < 0) \end{cases} \tag{4}$$

Considering $A + B = 1$, this equation set can be rewritten as follow.

$$\begin{cases} \dfrac{\sigma_{f,t}}{\tau_f + \sigma_{f,t}}\tau_m + \dfrac{\tau_f}{\tau_f + \sigma_{f,t}}\sigma_1 = \dfrac{\sigma_{f,t}\tau_f}{\tau_f + \sigma_{f,t}} & (\sigma_1 \geq 0) \\ \dfrac{\sigma_{f,c}}{\tau_f + \sigma_{f,c}}\tau_m + \dfrac{\tau_f}{\tau_f + \sigma_{f,c}}\sigma_1 = \dfrac{\sigma_{f,c}\tau_f}{\tau_f + \sigma_{f,c}} & (\sigma_1 < 0) \end{cases} \tag{5}$$

Then,

$$\begin{cases} A = \dfrac{\sigma_{f,t}}{\tau_f + \sigma_{f,t}}, B = \dfrac{\tau_f}{\tau_f + \sigma_{f,t}}, D_f = \dfrac{\sigma_{f,t}\tau_f}{\tau_f + \sigma_{f,t}} \ (\sigma_1 \geq 0) \\ A = \dfrac{\sigma_{f,c}}{\tau_f + \sigma_{f,c}}, B = \dfrac{\tau_f}{\tau_f + \sigma_{f,c}}, D_f = \dfrac{\sigma_{f,c}\tau_f}{\tau_f + \sigma_{f,c}} \ (\sigma_1 < 0) \end{cases} \quad (6)$$

The constants of *A, B* and D_f are now expressed in the terms of fracture/critical principal stress and maximum shear stress, which can be readily determined experimentally. In the case of CWR, the first principal stress σ_1 is always positive. Therefore, these three material constants can be determined by only two simple tests (pure shear test, and uniaxial tensile test).

Therefore, the limited number of material constants along with easy methods to determine their values offer the industry the maximum convenience and efficiency to produce central crack free products. This criterion is proposed based on the specific stress state in the CWR process. However, it is expected that it is applicable to other metal forming processes that generate a stress state in the workpiece with similar characteristics and history. Research is being undertaken to test its applicability in other applications.

2.4 Other central cracks criteria

A large number of fracture criteria or damage models are available in literature for the prediction of central crack formation in CWR. The accuracy of Cockcroft and Latham (C&L) damage model was proved by Pater (2014) and Zhou et al. (2014), respectively. Novella et al., (2015) modified Oyane model and experimentally predicted its accuracy taking into account of the temperature and strain rate. These mentioned models were proved to be able to predict the location of fracture and when the central cracks happen in a few cases, but it is still doubtful whether they can accurately predict the central crack occurrence in a set of CWR processes with various die geometries. Li (2003) experimentally studied that the plastic strain criterion was able to predict the trend of central crack formation for various die geometries, the robustness is necessary to be proved again. Rice and Tracey (R&T) damage model as the fundamental micromechanical model along with a wide application in industry could be able to predict the central crack formation given the commonly acknowledged ductile fracture nature of central cracks in CWR. The equations describing these models are shown in Table 2.

Table 2

Four typical fracture criteria or damage models.

Fracture criteria or damage models	Equations	
Maximum plastic strain criterion (Li and Lovell, 2004)	$\bar{\varepsilon}_f = C$	$\bar{\varepsilon}_f$ - Plastic strain to fracture C - Critical damage value

Cockcroft and Latham model (Pater, 2014)(Zhou et al., 2014)	$\int_0^{\overline{\varepsilon_f}} \sigma^* d\bar{\varepsilon} = C$	σ^* - Maximum tensile stress
Rice and Tracey model (Rice and Tracey, 1969)	$\int_0^{\overline{\varepsilon_f}} \exp(1.5 * \frac{\sigma_m}{\bar{\sigma}}) d\bar{\varepsilon} = C$	σ_m - Hydrostatic stress $\bar{\sigma}$ - Equivalent stress
Oyane model (Novella et al., 2015)	$\int_0^{\overline{\varepsilon_f}} (1 + \frac{\sigma_m}{A_0 \bar{\sigma}}) d\bar{\varepsilon} = C$	A_0 - Material constant

Therefore, four damage models were selected and investigated in detail to further study their accuracy when predicting the central crack formation in CWR and compared with the proposed fracture criterion.

3. Results and discussion

3.1 Stress analysis in CWR

Complicated stress and strain behaviours are found in the workpiece during the CWR process. The Von Mises stress and equivalent plastic strain qualitative and quantitative analysis, on eight points along the radial direction (P1 - P4) and axial direction (P5 - P8), are revealed in Fig. 3 (obtained through simulating case 3 in Table 1). Note that P1-8 are initially evenly distributed before rolling. The non-uniform spatial distribution at the final position of the CWR, as seen in Fig. 3, indicates the severe heterogeneous deformation occurred on these eight points. The overall effective stress and strain are generally increasing with the CWR process, given some fluctuations and cyclic variations are found near the free surface due to the rotation of the workpiece. Along the axial direction, the central point P1 tends to accumulate higher effective stress and strain (~130 MPa, ~0.7) compared to the points toward the side ends of the workpiece e.g. P5-8 (~120 MPa and ~0.4). However, the stress and strain at the central point are much lower than the points adjacent to the outer surface of the workpiece P2-4 (160 MPa and 3.25). This indicates large plastic deformation occurs near the free surface of the workpiece, and due to the stretching stress along the axial direction, the central interior region is imposed with higher deformation than the points near the side ends. Note that the central point P1 is neither the highest effective stress nor strain points during the CWR process. It implies more detailed analyses of the stress and strain states are required to understand the mechanistic crack formation process.

The exact stress and strain states in the tensor forms under the free surface and the middle central point during the CWR process (Case 3 in Table 1) are interrogated and shown in Fig. 4. The stress and strain components vary in a more complex form than the effective stress and strain seen in Fig. 3, particularly for the point near the

free surface of the workpiece due to the workpiece rotation. Large in-phase and out-phase oscillations between tensile and compression exist in almost all stress and strain components.

The stress and strain state variations are in a simpler form at the central point. However, the terms of stress and strain are still complex to interpret. The predominate stress terms σ_{xx} and σ_{yy} of the middle central point of the workpiece (Fig. 4(c)) are under tension along the axial and radial direction, while the σ_{zz} and shear stress σ_{zx} are in compression state and their magnitudes are relatively smaller. Further, the strain components generated at the centre (Fig.4 (d)), follow a similar trend as stresses with some minor fluctuations for ε_{yy} and ε_{zz} due to the workpiece rotation. Note, that the peak value of the axial stress and strain are found at different stages. The peak strain along the axial direction of 0.9 is found near the end of the rolling process i.e. at the sizing stage (in Fig.4 (d)), so is the highest stress as shown in Fig.4 (c).

Therefore, based on the stress-strain analyses, it can be concluded that on the transverse section of the workpiece, the surface subjected to the largest plastic deformation and material flow, while at the central region, large axial and radial tension presents.

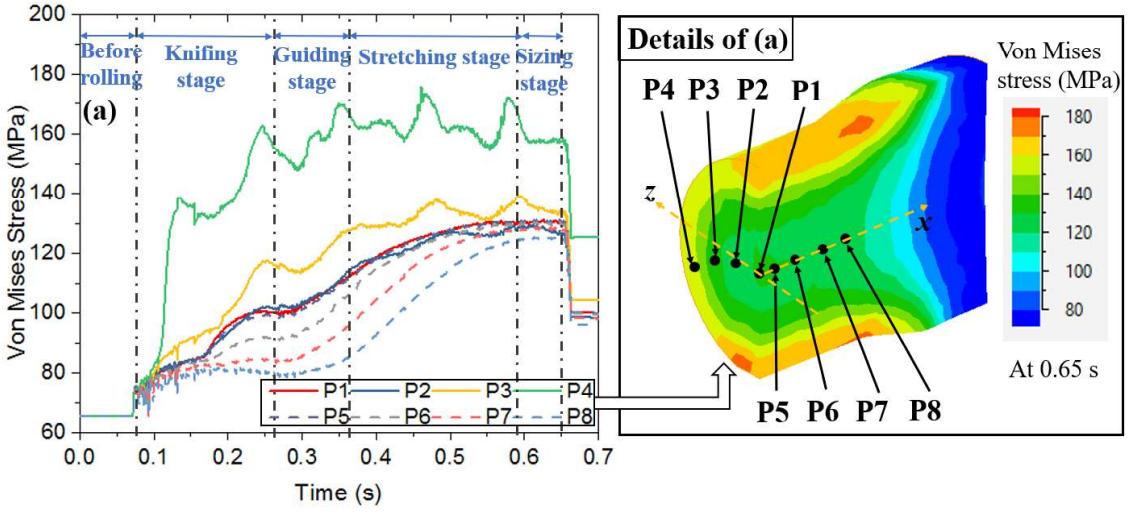

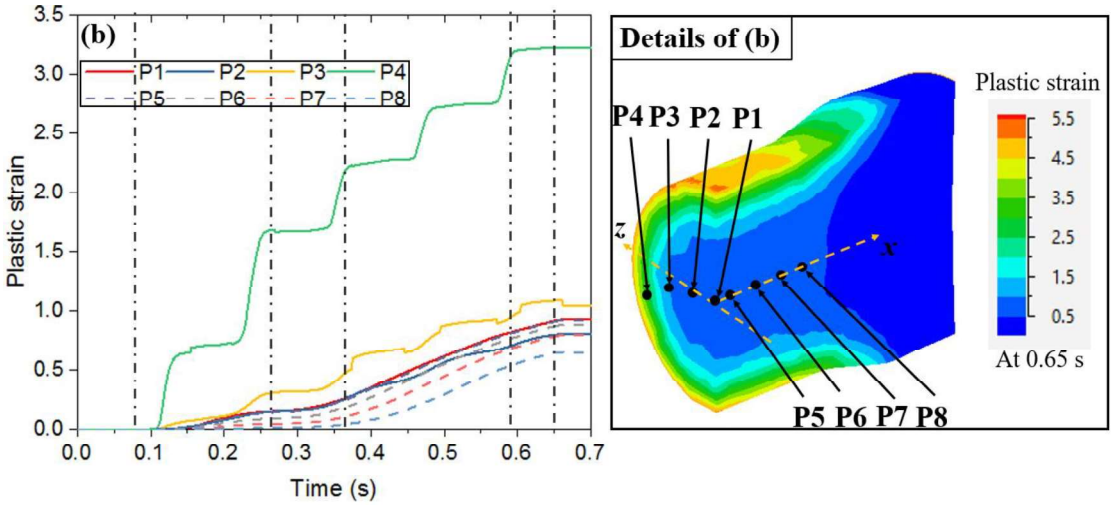

Fig. 3. Stress and strain distributions on the workpiece along the radial and axial direction during CWR (a) Von Mises stress; (b) Equivalent plastic strain.

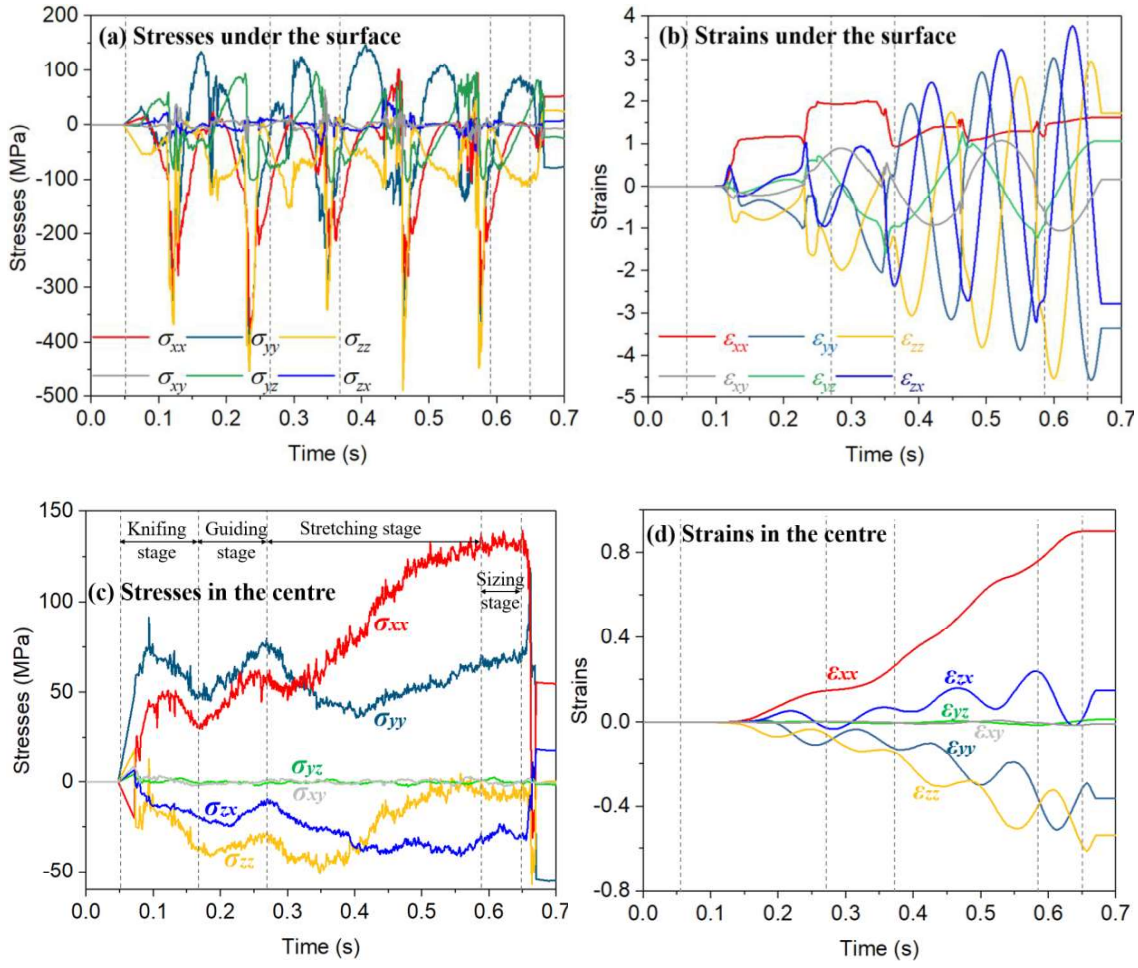

Fig. 4. Stress and strain evolution on the surface and in the centre in CWR: (a)(b) Stress and strain tensors under the surface; (c)(d) Stress and strain tensors in the centre.

3.2 Verification of novel fracture criterion

All 27 experimental tests of dies and the CWR processes were simulated by QForm. To demonstrate the variation and evolution of existing damage criterion (accumulated plastic strain and C&L model) during the CWR at the middle central point, 4 representative cases were selected and shown in Fig. 5 (a) and (b), for which the first two cases (case 2 and case 3) cracked and case 1 and case 7 did not crack. The damage values based on the selected cases keep increasing during the CWR and reach the peak value at the end of the CWR. This is expected as these two failure models are strain or energy accumulated damage models. It is clear that these models are not appropriate to predict the central crack formation. For example, case 7 which has the highest plastic strain and C&L damage value among the four cases, did not crack.

A more quantitative investigation was conducted to look at all 27 cases with all four commonly used fracture criteria. These criteria are found to be accurate to some extent, however, none of them seems to be able to reliably

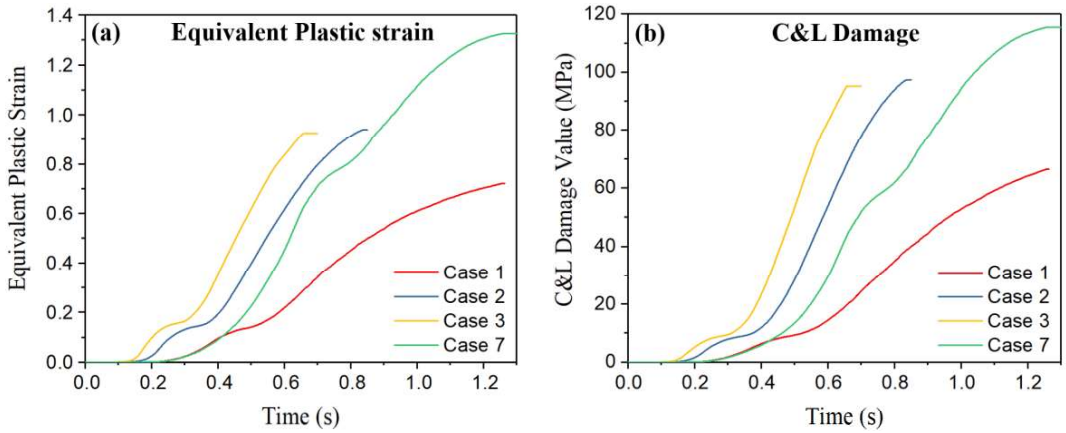

Fig. 5. Details of damage evolution of 4 selected cases performed under different damage models: (a) Maximum plastic strain criterion; (b) C&L damage model.

predict (>80% accuracy) whether the central crack will form for a given die geometry. The statistical results are presented in Fig. 6, for which the *x*-axis represents the case number and the *y*-axis shows the highest damage value found during the CWR for the given die geometry. Black dots represent no cracking found while the white dots represent cracking found after the CWR. If a reliable fracture model is found, a clear horizontal cut between the dark and white dots will be observed, as it indicates the critical damage value to differentiate the cracking and no-cracking cases. The dots are not randomly distributed as some patterns can be seen in these four plots. This is the result due to the systematic variation of the die parameters. However, the white and black dotes

are mixed up for all four failure criteria, and hence, no critical value can be determined. Therefore, these four damage models are not suitable for the prediction of central cracks in CWR routine.

The maximum strain criterion integrates the equivalent plastic strain ($\bar{\varepsilon}^p = \int \sqrt{\frac{2}{3} d\varepsilon_{ij}^p d\varepsilon_{ij}^p}$) during the deformation process. However, the signs of the strains (tensile or compressive) are not distinguished in this model. Hence, for deformation involving oscillating tensile and compressive strains, as in CWR, it is difficult to accurately predict fracture. The C&L damage model is energy-based and integrates the maximum tensile stress and the equivalent plastic strain. This damage model is based upon the first principal stress, which ignores the effect of the large radial compression that occurs in CWR. The R&T model is based upon the relation between stress triaxiality and micro-void growth leading to fracture; this model does not consider the process of void nucleation. The Oyane damage model combines the effects of accumulated strain and stress triaxiality. It also considers void nucleation and coalescence; however, it does not take into account the effect of radial compression generated during CWR that would accelerate the fracture process.

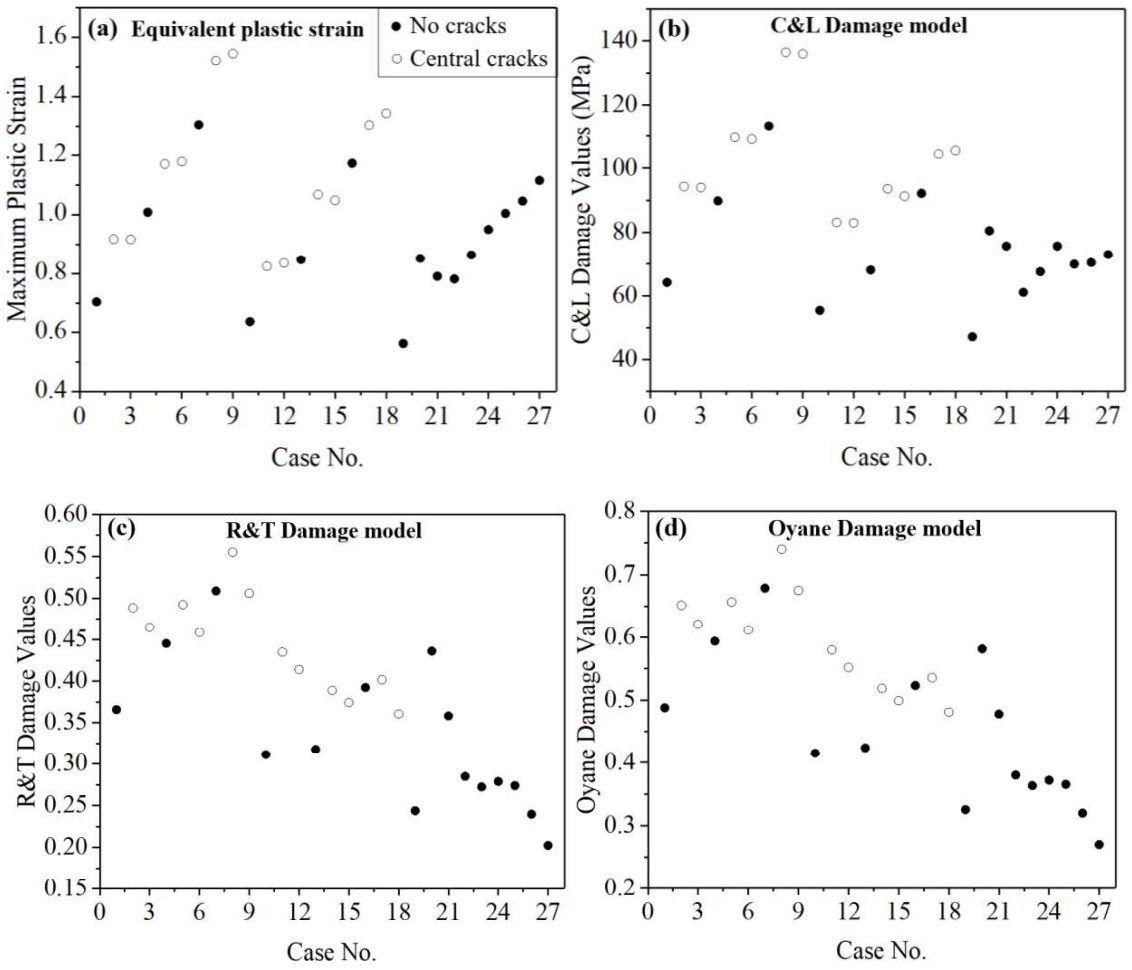

Fig. 6. Results of damage distributions of 27 cases simulated using different damage model (a) equivalent plastic strain; (b) C&L damage model; (c) R&T damage model; (d) Oyane damage model.

The limitations mentioned above might be due to the lack of understanding of the actual fracture mechanism in CWR. For example, the effect of shear stress, which has been shown to have a significant effect on central crack formation as indicated by Li et al. (2002) and/or Yang et al. (2018), is not considered by any of these models.

Through the analyses of the complicated stress and strain state distribution and evolution during the CWR, and the thorough comparison of the effects of three key die geometrical parameters on central crack formation in all 27 cases, a new failure criterion is proposed and shown in Section 2.3. It is proposed that the central crack formation is mainly driven by the combined effects of the first principal stress and shear stress. It can be expressed in a formed of $D = A\tau_m + B\sigma_1$ as seen in Eq. 2.

A high accuracy is achieved using the newly proposed criterion to predict the central cracking in all 27 cases. As presented in Fig. 7(a), in contrary to previous failure criteria, dark and white dots are clearly separated using this new principal and maximum shear stress-based criterion. A line can now be drawn to determine all cracked and no cracked cases among all 27 cases. The critical damage value is defined and normalised as 1 for easy comparison between different materials. Take a closer look at the damage evolution of this new criterion by revisiting the previously selected four specific cases, namely, case 1, 2, 3 and 7. In Fig. 7(b), the calculated damage value is shown in the function of processing time. The highest damage values for each case are ranked correctly. For example, the cracked case 2 and 3 displayed higher damage values than the no cracked case 1 and 7. Especially, case 7 previously incorrectly predicted the highest damage value among these four cases is predicted correctly by using the new criterion. It is also interesting to note that the peak damage values do not always occur at the end of the process, in some cases, the high damage value is found in the knifing or stretching zone. Furthermore, the first principal stress σ_1 is changing its direction. Initially, its direction is along the radial (y) compression direction during the knifing stage. This direction changes to the axial (x) direction during the stretching stage where the axial extension is predominated (see details of Fig. 7(c)). Case 3 was considered as an example to show the evolution of the stress components and its damage values during CWR as Fig. 7(c) that the first principal stress σ_1 increases in the knifing portion, and has some slight fluctuations during the next stage, after which, it increases significantly and researches the highest value at the end of the whole process. The maximum shear stress τ_{max} was calculated by$(\sigma_1 - \sigma_3)/2$ and was noted a constant increase in its value until to

the end of stretching stage. Further, the proposed damage model exhibits a similar trend as that of τ_{max}. The maximum damage value in case 3 exceeds the critical value of 1 at the end of the stretching stage, thus confirming the occurrence of the central crack.

Only three material constants (A, B and D_f) exist in the new damage model. The values of these three constants in this study are obtained through data fitting of the 27 experimental cases, in which the damage value calculated based on these three constants should clearly discriminate the cracked and none cracked cases. The values were determined as: A= 0.94, B = 0.06, and D_f = 77.64 MPa, as parameters used in Eq (8). The numerical values (A and B) determined for the proposed model indicate this material during CWR is a shear stress dominant fracture, while the first principal stress is acting of accelerating the shear fracture, which is consistent with the findings made by Yang et al. (2018) and later by Yamane et al. (2019).

$$D = 0.94\tau_m + 0.06\sigma_1 \begin{cases} \geq 77.64 \text{ MPa} & \text{Central Crack} \\ < 77.64 \text{ MPa} & \text{No crack} \end{cases} \quad (8)$$

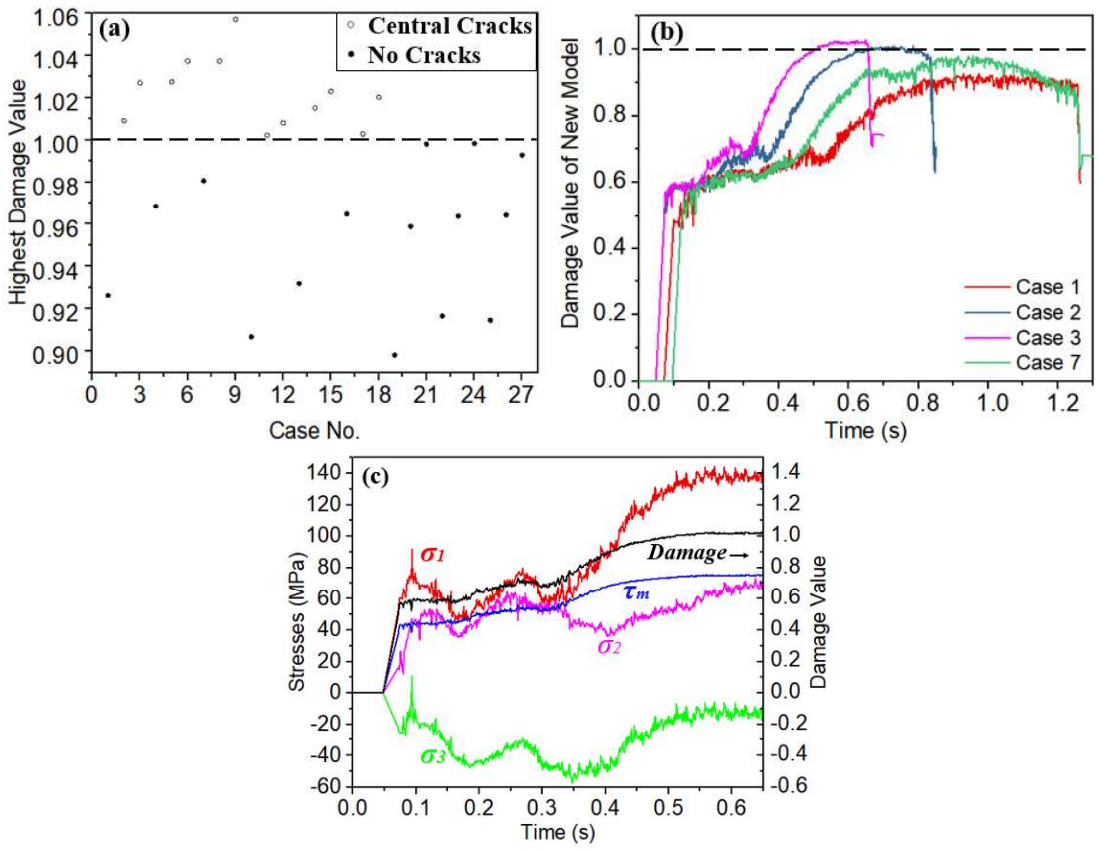

Fig. 7. Details of damage evolution and distribution generated using the novel fracture criterion (a) Fracture distribution of 27 cases; (b) Damage evolution of 4 cases; (c) Stress components and damage evolution as a function of time for the case 3.

The predicted damage morphology at the transverse and longitudinal section of the workpiece is in an excellent agreement with experimentally observed fracture morphology. The comparison is shown in Fig. 8, indicating the high level of accuracy of this new damage model.

3.3 Fracture mechanisms of central formation in CWR

The new damage model expects to work for both shear and principal stress-driven fracture. These two failure modes can occur in the central region of the workpiece during CWR depending on the material properties and the designed die geometry. Materials (e.g. Al 1100 and AISI 1045) submitted to the CWR show the evidence of void growth and coalescence in the central region as observed by Li and Lovell (2004), Huo et al. (2017) and Yang et al. (2018). Therefore, the fracture mechanism was assumed to be ductile fracture. However, with different materials or stress states, it is possible to be brittle fracture, especially, during the crack propagation process. Therefore, in this study, it is assumed that both fracture mechanisms exist, and they interact mutually.

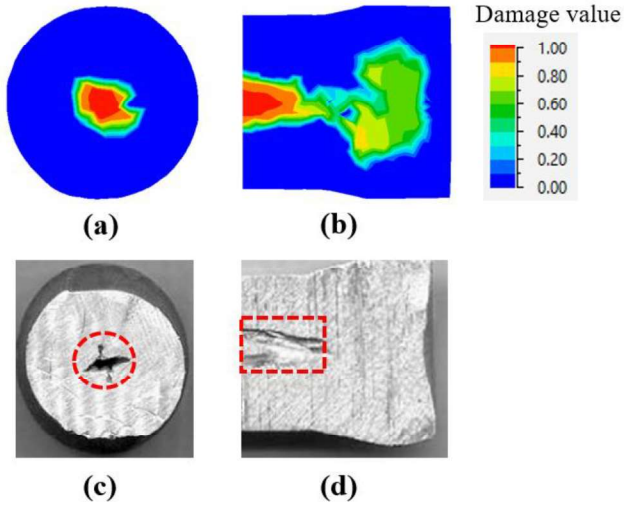

Fig. 8. Patterns of fracture location from the simulation results and experimental process (a) transverse section of simulated result; (b) longitudinal section of simulated result; (c) transverse section of experimental result (Li et al., 2002); (d) longitudinal section of experimental result (Li et al., 2002).

The speculated fracture mechanism of the central crack in CWR is illustrated in Fig. 9. This is based on the stress and damage analyses presented in Section 3.1 and 3.2. In Fig. 3 (c), it can be seen that the maximum shear stress at the stretching stage is on the transverse plane, allowing the void nucleation on the shear bands as the red lines shown in Fig. 10(a). After voids nucleation, the voids propagate quickly due to the combined efforts of

the normal stresses σ_{yy} and σ_{zz} and the shear stress σ_{zy}. The cyclic normal stresses (from compressive to tensile stress or from tensile to compressive stress) caused by the workpiece rotation enable the ends of voids sharper. The shear stress σ_{zy} keeps increasing at the beginning of the stretching stage, increasing the ovality of the voids, followed by the strong stress localisation at the ends of the voids. Once sharp ends are formed, these voids can propagate, and coalescence very quickly and finally form macrocracks as shown in Fig. 9 (b) and (c). This agrees well with our predicted damage value morphology at the transverse and longitudinal section as seen in *Fig. 8*. Note that, though the crack nucleation and propagation process is similar to the typical GNT model proposed by Gurson (1977) and further developed by Needleman and Tvergaard (1984), the driving factors for crack nucleation and propagation are completely different in the CWR case.

On the longitudinal section, the voids are growing in a distinct way compared to the transverse section. The voids are elongated along the axial direction due to the presence of large axial stress. Meanwhile, the maximum shear stress transfers to the longitudinal plane, which accelerates the void nucleation as well as the propagation of the existed voids. Then, the micro-voids form near the tips of the original voids and propagates through a specific path as indicated by the red lines in Fig. 9 (b) and (c). Anderson (2012) noted that the crack propagation path may

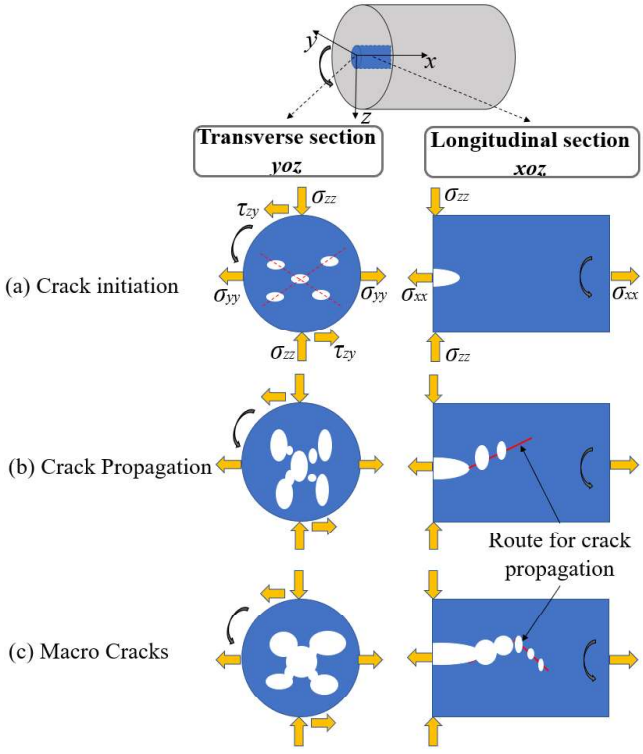

Fig. 9. Schematics of fracture mechanisms patterns of central cracks produced by the CWR: (a) Crack initiation; (b) Crack propagation; (c) Macro cracks.

form approximately at the 45° degrees with the axial direction of the workpiece, which depends on the material property and the ratio of axial stress and radial stress. Once the workpiece rotates, the shear bands start to vary, generating a new crack path that always propagates along the axial direction.

In short, the microcracks initiate on the shear bands due to the maximum shear stress on the transverse plane at the stretching stage. The cyclic loadings and increasing shear stress accelerate crack propagation. On the longitudinal section, the workpiece rotation can control the propagation path.

In literature, it is argued by Fu and Dean (1993) that the stress/strain reversals might be the reason for void nucleation, different from the fracture mechanism proposed here. The rotary swaging process is a good example to support that reversal stress/strain is not the prerequisite condition for central crack formation. This process is another competing manufacturing technique for producing axle-shaped components, in which axle parts are continuously subjected to cyclic reversed swaging as studied by Rong et al. (2007), but in this process no central crack formation is found in its products, suggesting there is more to the failure than only stress/strain reversals.

Experiments are being conducted to prove the proposed fracture mechanisms by replicating the stress states in CWR as well as the crack nucleation and propagation process.

4. Conclusions

In this study, a new shear stress driven fracture criterion is proposed to predict the central crack occurrence in the CWR. 27 rigorous experimental CWR cases with various die geometries have been simulated by QForm to investigate material response in the CWR. Complete knowledge of the stress, strain states and evolution through the CWR process was obtained and the key factors influencing the central crack formation have been identified. The main findings can be summarized as:

1) Two stress components (the first principal stress and maximum shear stress) have been identified to be important to central crack formation. The highest first principal stress occurs in the central region, while the maximum shear stress in the central region is accumulating during the CWR process.

2) The maximum shear stress driven central crack formation is found for Al 1100, CWR at room temperature. Void nucleation is caused by the maximum shear stress assisted with the longitudinal stress. The crack propagation is accelerated by the normal stresses (cyclic stresses on the transverse plane and axial normal stress on the longitudinal plane).

3) The maximum shear and first principal stress-driven fracture criterion is proposed based on the Tresca and first principal criterion along with the fundamental understanding of fracture mechanisms in CWR. Compared with the other four studied fracture criterion or damage models, this proposed criterion shown improved accuracy in all 27 CWR cases.

Acknowledgements

The authors thank the financial support from Imperial-AVIC research centre and Royal Society-Newton Mobility Grant. Xianyan Zhou acknowledges the Chinese Scholarship Council (Grant number: 201606950020) for her bursary.

References

Anderson, T.L., 2012. Fracture Mechanics: Fundamentals and Applications, Taylor & Francis Group. https://doi.org/10.1016/j.jmps.2010.02.008

Cao, T.S., Bobadilla, C., Montmitonnet, P., Bouchard, P.O., 2015. A comparative study of three ductile damage approaches for fracture prediction in cold forming processes. J. Mater. Process. Technol. 216, 385–404. https://doi.org/10.1016/j.jmatprotec.2014.10.009

Fu, X.P., Dean, T.A., 1993. Past developments, current applications and trends in the cross wedge rolling process. Int. J. Mach. Tools Manuf. 33, 367–400. https://doi.org/10.1016/0890-6955(93)90047-X

Gurson, A.L., 1977. Continuum Theory of Ductile Rupture by Void Nucleation and Growth: Part I—Yield Criteria and Flow Rules for Porous Ductile Media. J. Eng. Mater. Technol. 99, 2. https://doi.org/10.1115/1.3443401

Hu, Z., Wang, B., Zheng, Z., 2018. Research and industrialization of near-net rolling technology used in shaft parts. Front. Mech. Eng. 13, 17–24. https://doi.org/10.1007/s11465-018-0480-3

Hu, Z., Yang, C., Wang, B., 2012. Development of part rolling technology in China. Jixie Gongcheng Xuebao/Journal Mech. Eng. 48, 7–12. https://doi.org/10.3901/JME.2012.18.007

Hu, Z., Zhang, K., Wang, B., 1995. Forming technology and simulation of cross wedge rolling.

Huo, Y., Lin, J., Bai, Q., Wang, B., Tang, X., Ji, H., 2017. Prediction of microstructure and ductile damage of a high-speed railway axle steel during cross wedge rolling. J. Mater. Process. Technol. 239, 359–369. https://doi.org/10.1016/j.jmatprotec.2016.09.001

Komischke, T., Hora, P., Domani, G., 2018. A New Experimental Method for the Evaluation of Fracture Criteria in Bulk Forming Operations, in: Forming Technology Forum 2018. Zurich, pp. 65–69.

Lee, H.W., Lee, G.A., Yoon, D.J., Choi, S., Na, K.H., Hwang, M.Y., 2008. Optimization of design parameters using a response surface method in a cold cross-wedge rolling. J. Mater. Process. Technol. 201, 112–117. https://doi.org/10.1016/j.jmatprotec.2007.11.287

Lemaitre, J., 1985. A Continuous Damage Mechanics Model for Ductile Fracture. J. Eng. Mater. Technol. 107, 83–89. https://doi.org/10.1115/1.3225775

Li, Q., 2003. Characterization of failure mechanisms in cross wedge rolling. University of Pittsburgh.

Li, Q., Lovell, M.R., 2004. The establishment of a failure criterion in cross wedge rolling. Int. J. Adv. Manuf. Technol. 24, 180–189. https://doi.org/10.1007/s00170-003-1607-0

Li, Q., Lovell, M.R., Slaughter, W., Tagavi, K., 2002. Investigation of the morphology of internal defects in cross wedge rolling. J. Mater. Process. Technol. 125–126, 248–257. https://doi.org/10.1016/S0924-0136(02)00303-5

Li, Z., Shi, J., Tang, A., 2014. Investigation on fracture mechanisms of metals under various stress states. Acta Mech. 225, 1867–1881. https://doi.org/10.1007/s00707-013-1024-x

Madou, K., Leblond, J., 2012. Journal of the Mechanics and Physics of Solids A Gurson-type criterion for porous ductile solids containing arbitrary ellipsoidal voids — I : Limit-analysis of some representative cell. J. Mech. Phys. Solids 60, 1020–1036. https://doi.org/10.1016/j.jmps.2011.11.008

Mirahmadi, S.J., Hamedi, M., Ajami, S., 2014. Investigating the effects of cross wedge rolling tool parameters on formability of Nimonic® 80A and Nimonic® 115 superalloys. Int. J. Adv. Manuf. Technol. 74, 995–1004. https://doi.org/10.1007/s00170-014-6047-5

Nahshon, K., Hutchinson, J.W., 2008. Modification of the Gurson Model for shear failure. Eur. J. Mech. A/Solids 27, 1–17. https://doi.org/10.1016/j.euromechsol.2007.08.002

Needleman, A., Tvergaard, V., 1984. An analysis of ductile rupture in notched bars. J. Mech. Phys. Solids 32, 461–490. https://doi.org/10.1016/0022-5096(84)90031-0

Novella, M.F., Ghiotti, A., Bruschi, S., Bariani, P.F., 2015. Ductile damage modeling at elevated temperature applied to the cross wedge rolling of AA6082-T6 bars. J. Mater. Process. Technol. 222, 259–267. https://doi.org/10.1016/j.jmatprotec.2015.01.030

Pater, Z., 2014. Cross-Wedge Rolling, Comprehensive Materials Processing. Elsevier. https://doi.org/10.1016/B978-0-08-096532-1.00315-0

Pater, Z., 1997. Theoretical method for estimation of mean pressure on contact area between rolling tools and workpiece in cross wedge rolling processes. Int. J. Mech. Sci. 39, 233–243.

Pater, Z., Tomczak, J., Bulzak, T., Bartnicki, J., Tofil, A., 2019. Prediction of Crack Formation for Cross Wedge Rolling of Harrow Tooth Preform. Materials (Basel). 12, 2287. https://doi.org/10.3390/ma12142287

Rice, J.R., Tracey, D.M., 1969. On the ductile enlargement of voids in triaxial stress fields∗. J. Mech. Phys. Solids 17, 201–217. https://doi.org/10.1016/0022-5096(69)90033-7

Rong, L., Nie, Z., Zuo, T., 2007. 3D finite element modeling of cogging-down rotary swaging of pure magnesium square billet-Revealing the effect of high-frequency pulse stroking. Mater. Sci. Eng. A 464, 28–37. https://doi.org/10.1016/j.msea.2007.01.086

Stebunov, S., Biba, N., Vlasov, A., Maximov, A., 2011. Thermally and mechanically coupled simulation of metal forming processes. Proc. 10th Int. Conf. Technol. Plast. ICTP 2011 2, 1–5.

Theoretical basis of QForm, 2017.

Wen, J., Huang, Y., 2005. The modified Gurson model accounting for the void size effect 21, 381–395. https://doi.org/10.1016/j.ijplas.2004.01.004

Wierzbicki, T., Bao, Y., Lee, Y.W., Bai, Y., 2005. Calibration and evaluation of seven fracture models. Int. J. Mech. Sci. 47, 719–743. https://doi.org/10.1016/j.ijmecsci.2005.03.003

Xue, L., Wierzbicki, T., 2008. Ductile fracture initiation and propagation modeling using damage plasticity theory 75, 3276–3293. https://doi.org/10.1016/j.engfracmech.2007.08.012

Yamane, K., Shimoda, K., Kuroda, K., 2019. New Ductile Fracture Criterion for Prediction of Internal Fracture

in Skew Rolling, in: XV International Conference on Computational Plasticity. Fundamentals and Applications.

Yang, C., Dong, H., Hu, Z., 2018. Micro-mechanism of central damage formation during cross wedge rolling. J. Mater. Process. Technol. 252, 322–332. https://doi.org/10.1016/j.jmatprotec.2017.09.041

Yu, M., 2002. Advances in strength theories for materials under complex stress state in the 20th Century. Appl. Mech. Rev. 55, 169. https://doi.org/10.1115/1.1472455

Zhou, J., Yu, Y., Zeng, Q., 2014. Analysis and experimental studies of internal voids in multi-wedge cross wedge rolling stepped shaft. Int. J. Adv. Manuf. Technol. 72, 1559–1566. https://doi.org/10.1007/s00170-014-5768-9

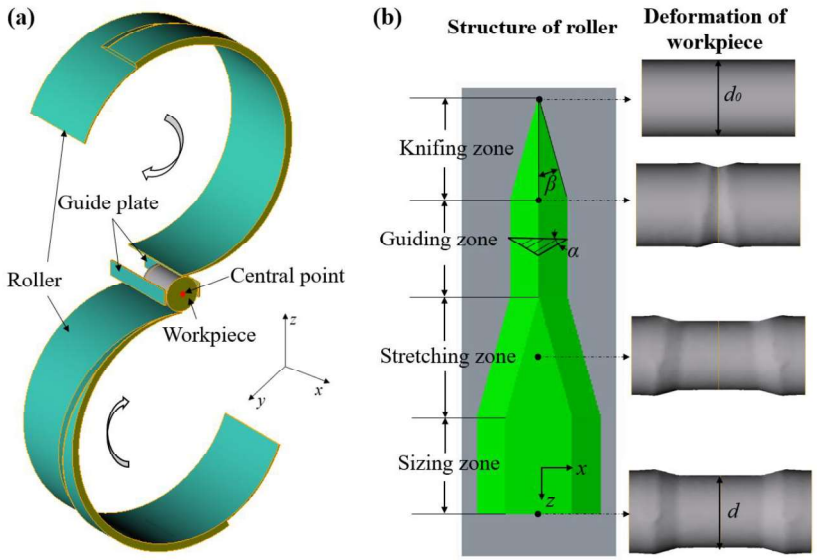

Fig. 1. The configuration of CWR (a) schematic of the modelled CWR process (b) configuration of the roller and the corresponding deformation stages during CWR.

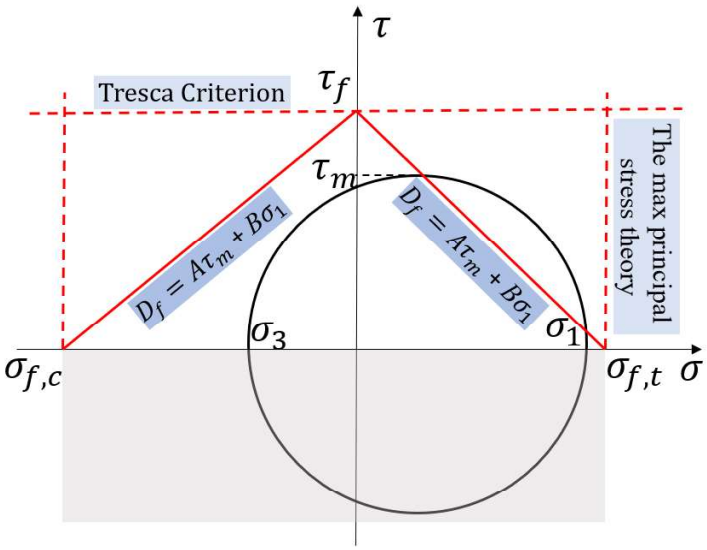

Fig. 2. Representation of fracture locus by the proposed criterion using the fracture lines and Mohr's circle.

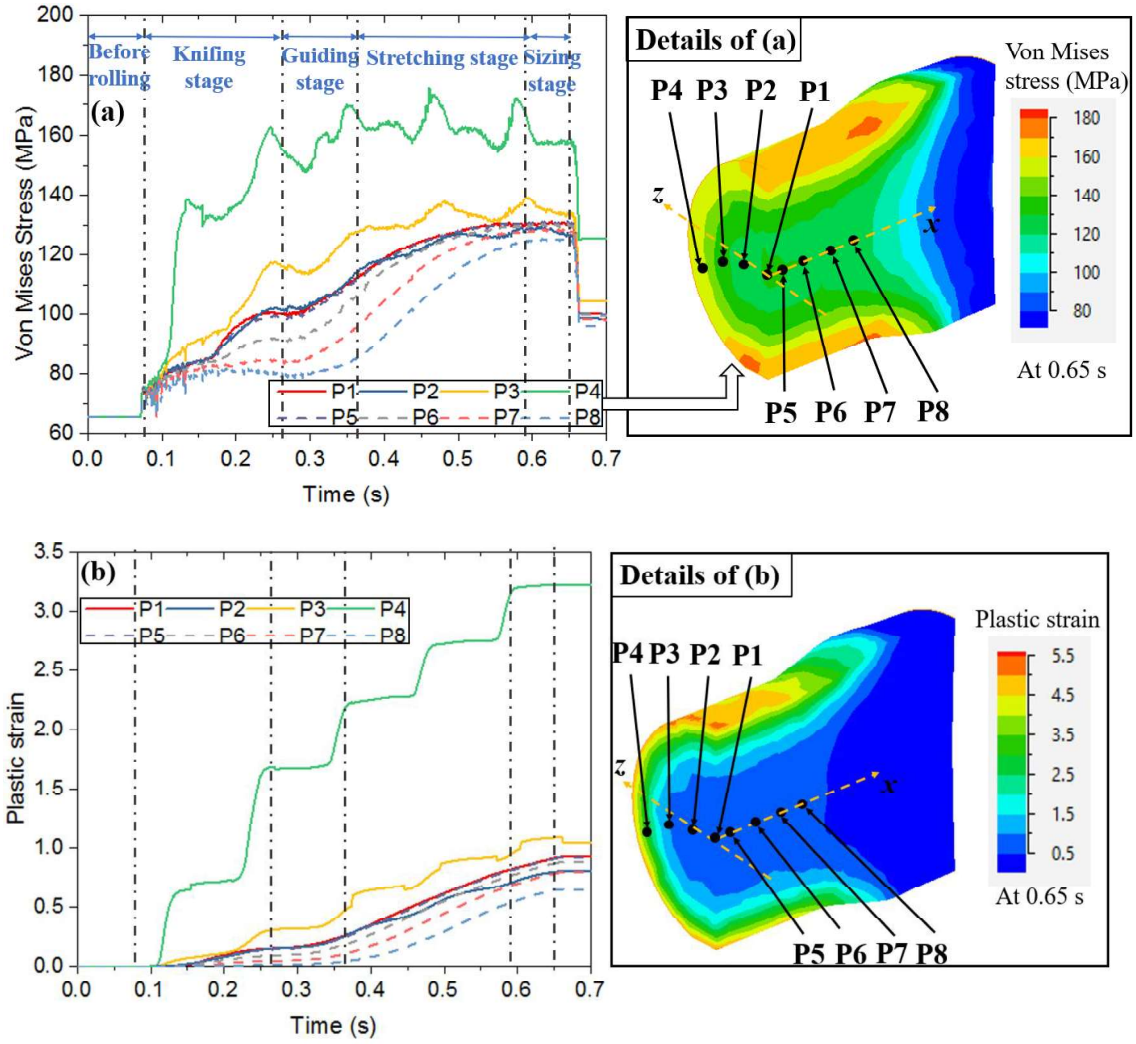

Fig. 3. Stress and strain distributions on the workpiece along the radial and axial direction during CWR (a) Von Mises stress; (b) Equivalent plastic strain.

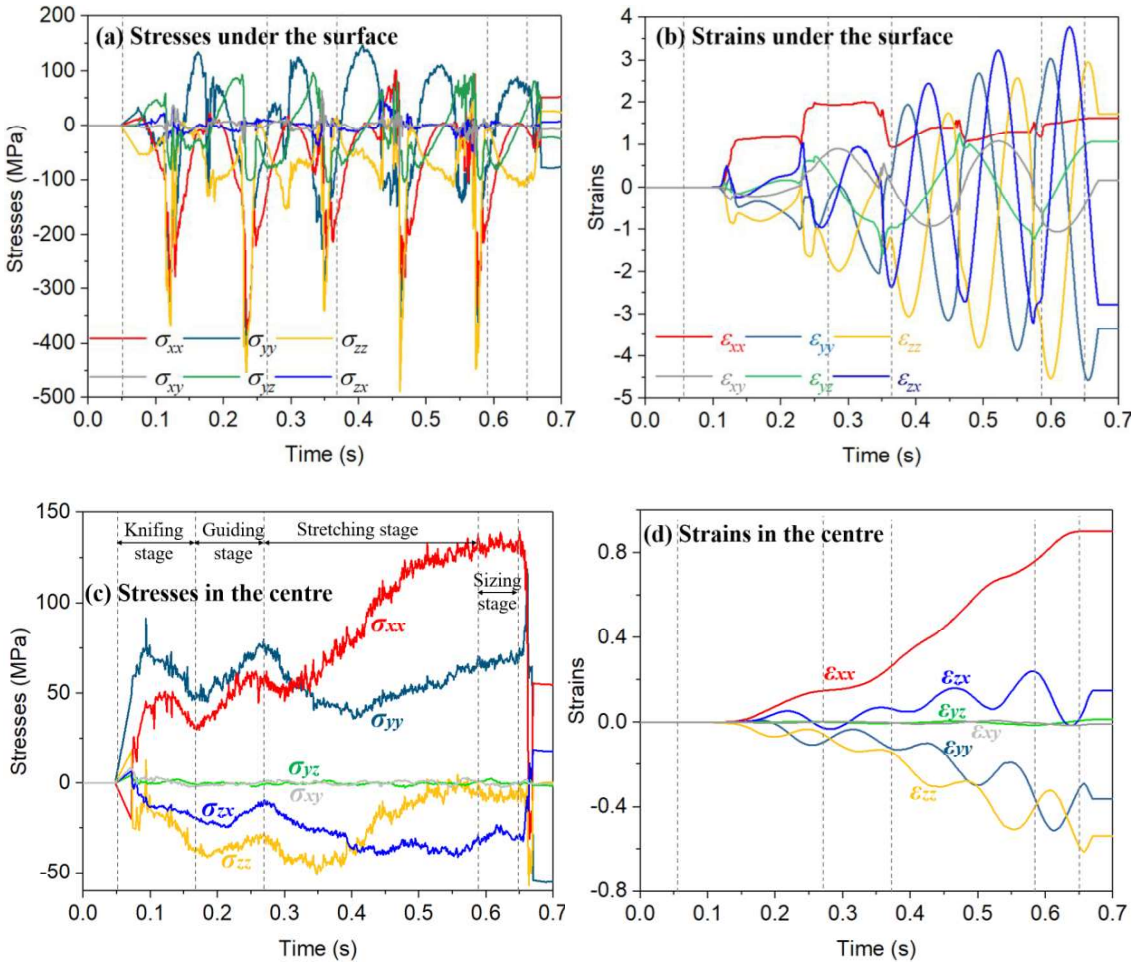

Fig. 4. Stress and strain evolution on the surface and in the centre in CWR: (a)(b) Stress and strain tensors under the surface; (c)(d) Stress and strain tensors in the centre.

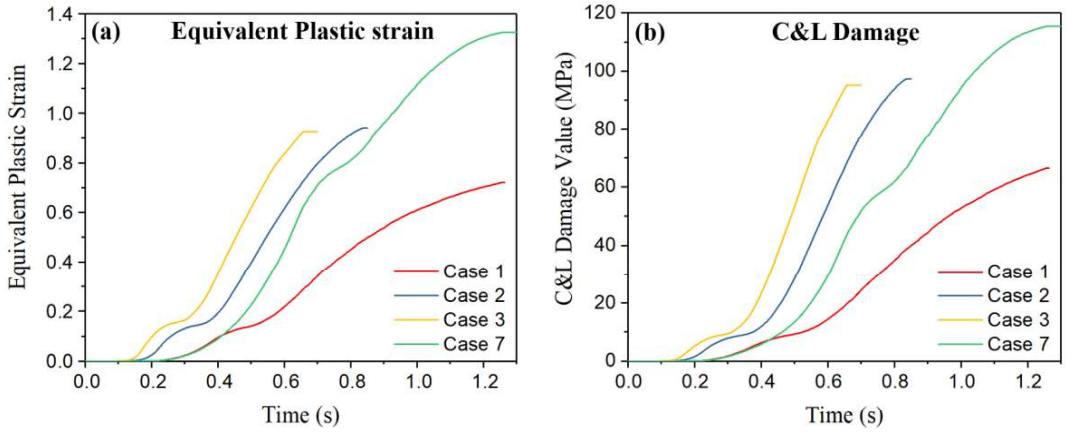

Fig. 5. Details of damage evolution of 4 selected cases performed under different damage models: (a) Maximum plastic strain criterion; (b) C&L damage model.

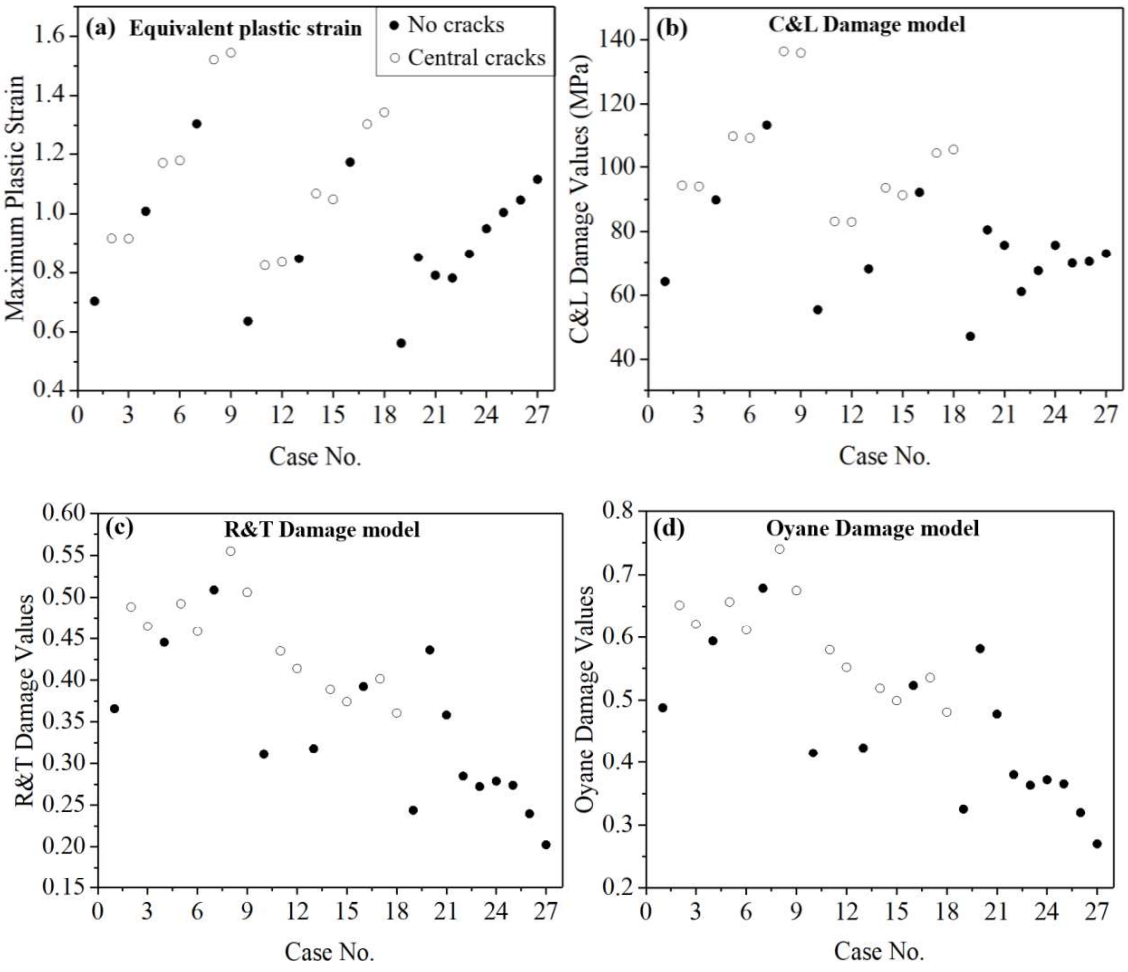

Fig. 6. Results of damage distributions of 27 cases simulated using different damage model (a) equivalent plastic strain; (b) C&L damage model; (c) R&T damage model; (d) Oyane damage model.

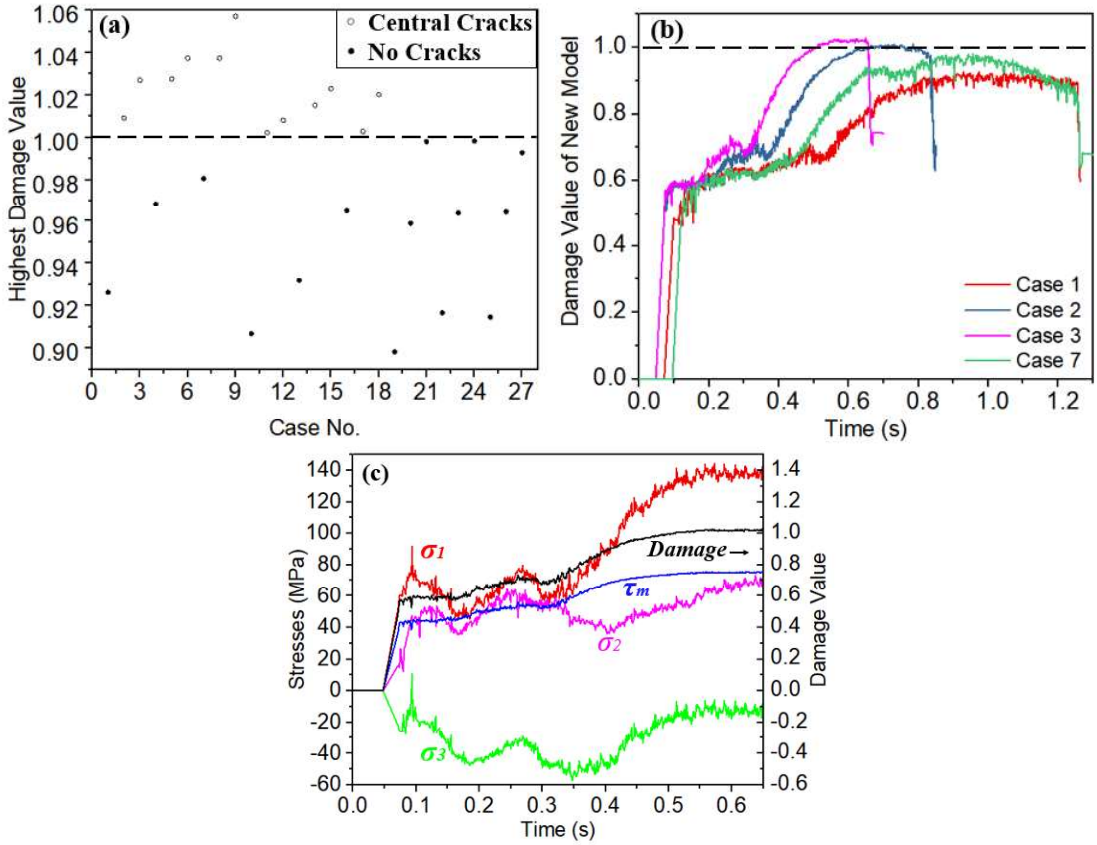

Fig. 7 Details of damage evolution and distribution generated using the novel fracture criterion (a) Fracture distribution of 27 cases; (b) Damage evolution of 4 cases; (c) Stress components and damage evolution as a function of time for the case 3.

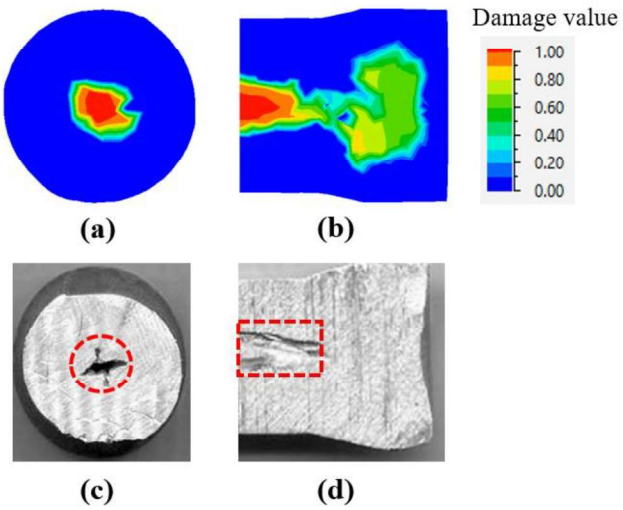

Fig.8. Patterns of fracture location from the simulation results and experimental process (a) transverse section of simulated result; (b) longitudinal section of simulated result; (c) transverse section of experimental result (Li et al., 2002a); (d) longitudinal section of experimental result (Li et al., 2002a).

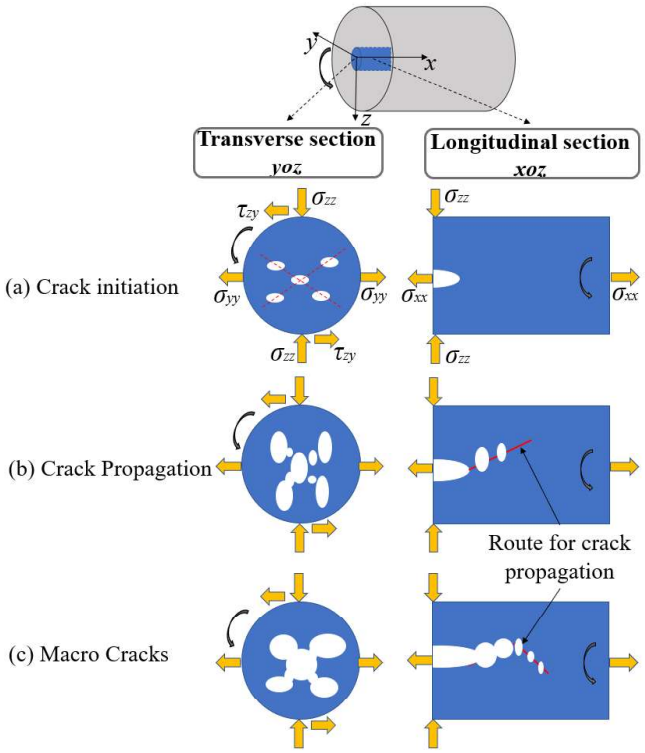

Fig. 9. Schematics of fracture mechanisms patterns of central cracks produced by the CWR: (a) Crack initiation; (b) Crack propagation; (c) Macro cracks.

Table 1.

Results of 27 CWR experiments considering various geometrical parameters (Li, 2003)(Li et al., 2002a).

Case Number	η	β (°)	α (°)	Experimental results
1	27	3	15	No crack
2	27	5	15	Central crack
3	27	7	15	Central crack
4	35	3	15	No crack
5	35	5	15	Central crack
6	35	7	15	Central crack
7	44	3	15	No crack
8	44	5	15	Central crack
9	44	7	15	Central crack
10	27	3	20	No crack
11	27	5	20	Central crack
12	27	7	20	Central crack
13	35	3	20	No crack
14	35	5	20	Central crack
15	35	7	20	Central crack
16	44	3	20	No crack
17	44	5	20	Central crack
18	44	7	20	Central crack
19	27	3	30	No crack
20	27	5	30	No crack
21	27	7	30	No crack
22	35	3	30	No crack
23	35	5	30	No crack
24	35	7	30	No crack
25	44	3	30	No crack
26	44	5	30	No crack
27	44	7	30	No crack

Table 2

Four typical fracture criteria or damage models.

Fracture criteria or damage models	Equations	
Maximum plastic strain criterion (Li and Lovell, 2004)	$\bar{\varepsilon}_f = C$	$\bar{\varepsilon}_f$ - Plastic strain to fracture C - Critical damage value
Cockcroft and Latham model (Pater, 2014)(Zhou et al., 2014)	$\int_0^{\overline{\varepsilon_f}} \sigma^* d\bar{\varepsilon} = C$	σ^* - Maximum tensile stress
Rice and Tracey model (Rice and Tracey, 1969)	$\int_0^{\overline{\varepsilon_f}} \exp(1.5 * \frac{\sigma_m}{\bar{\sigma}}) d\bar{\varepsilon} = C$	σ_m - Hydrostatic stress $\bar{\sigma}$ - Equivalent stress
Oyane model (Novella et al., 2015)	$\int_0^{\overline{\varepsilon_f}} (1 + \frac{\sigma_m}{A_0 \bar{\sigma}}) d\bar{\varepsilon} = C$	A_0 - Material constant